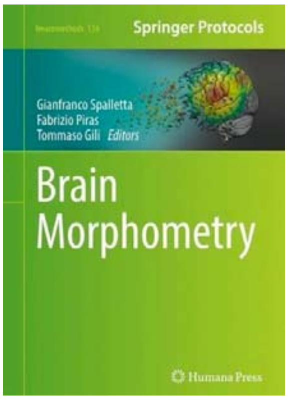

Brain Morphometry
(Neuromethods, Band 136)

Gianfranco Spalletta, Fabrizio Piras, Tommaso Gili

21. March 2018

Publisher: Humana Press; 1st ed. 2018 edition
ISBN-10: 1493976451
ISBN-13: 978-1493976454

Surface and Shape Analysis

Robert Dahnke[1] and Christian Gaser[1]

During evolution, the brain becomes more and more complex. With increasing volume, the surface area expands to a disproportionately greater extent through the development of a species-specific but individual folding pattern. As shaping of the brain is virtually complete in early development, this permits the adult brain to be the subject of shape analysis to investigate its development. Other surface properties such as thickness alter significantly over the entire lifetime and in diseases, and reflect the current state of the brain. This chapter offers an introduction to individual development theories and models, surface reconstruction techniques, and shape measures to describe surfaces properties.

Key words: surface, shape, measures, folding, gyrification, MRI, brain, thickness, curvature, development, aging, evolution, morphometry, structure

1. The mammalian brain 1
2. Brain development, plasticity, and aging 3
Phase I: ballooning 4
Phase II: gyrification 4
Phase III: further scaling 4
Adulthood and aging 4
Interim conclusion 4
3. Folding theories and models 4
4. Surface creation 5
4.1. Voxel-based preprocessing 5
4.2. Mesh generation 6
4.3. Mesh modification 6
4.4. Spatial normalization and spherical registration of meshes 6
4.5. Surface measures 6
4.6. Surface analysis (SBM) 8
4.7. Conclusion 10
References 10

1. The mammalian brain

The beginning of systematic studies of the human brain in the 19th century raised questions about the link between anatomical structure and its function and how obvious folding affects its abilities [1-9]. During evolution and development, the enlargement of the brain coincides with increased and more individual folding that comprises a non-linear enlargement of surface area that correlates with increased intellectual capabilities [6-9]. The individual shape of the brain, especially for larger species, requires nonlinear registration techniques to compare different brain structures [10-12]. Besides highly individual pattern folding, population- and disease-specific pattern have been found that are the product of early development [8,9,13-15].

The brain is arranged in two major classes of tissue, gray matter (GM) and white matter (WM), which are surrounded by cerebrospinal fluid (CSF) and packed within the skull (Figure 1A). The GM can be seen as the processing region with a large number of neurons that are connected by myelinated dendrites that form WM fiber tracts and allow high-speed connection between different regions. In contrast, CSF serves as a physical buffer that allows geometrical changes in brain development and aging. The surface area of the cortex, a strong folded ribbon of GM that surrounds the WM, is particularly increased during both individual and evolutional development [5-9,14] (Figure 1B and 1C). The cortex can be described as an organized surface whose folding allows a large surface to fit compactly within the cranium [7,13,16-18]. The gyrification process that creates outward (gyri) and inward (sulci) folding during embryogenesis is still under discussion [9,14,15,18,19]. The closer connectivity within the gyri and the obvious similarities in the folding pattern of smaller species and major structures led to the expectation that the gyri process related things [8,13,18]. The cortex of the cerebrum (neocortex) is organized into six layers with regional

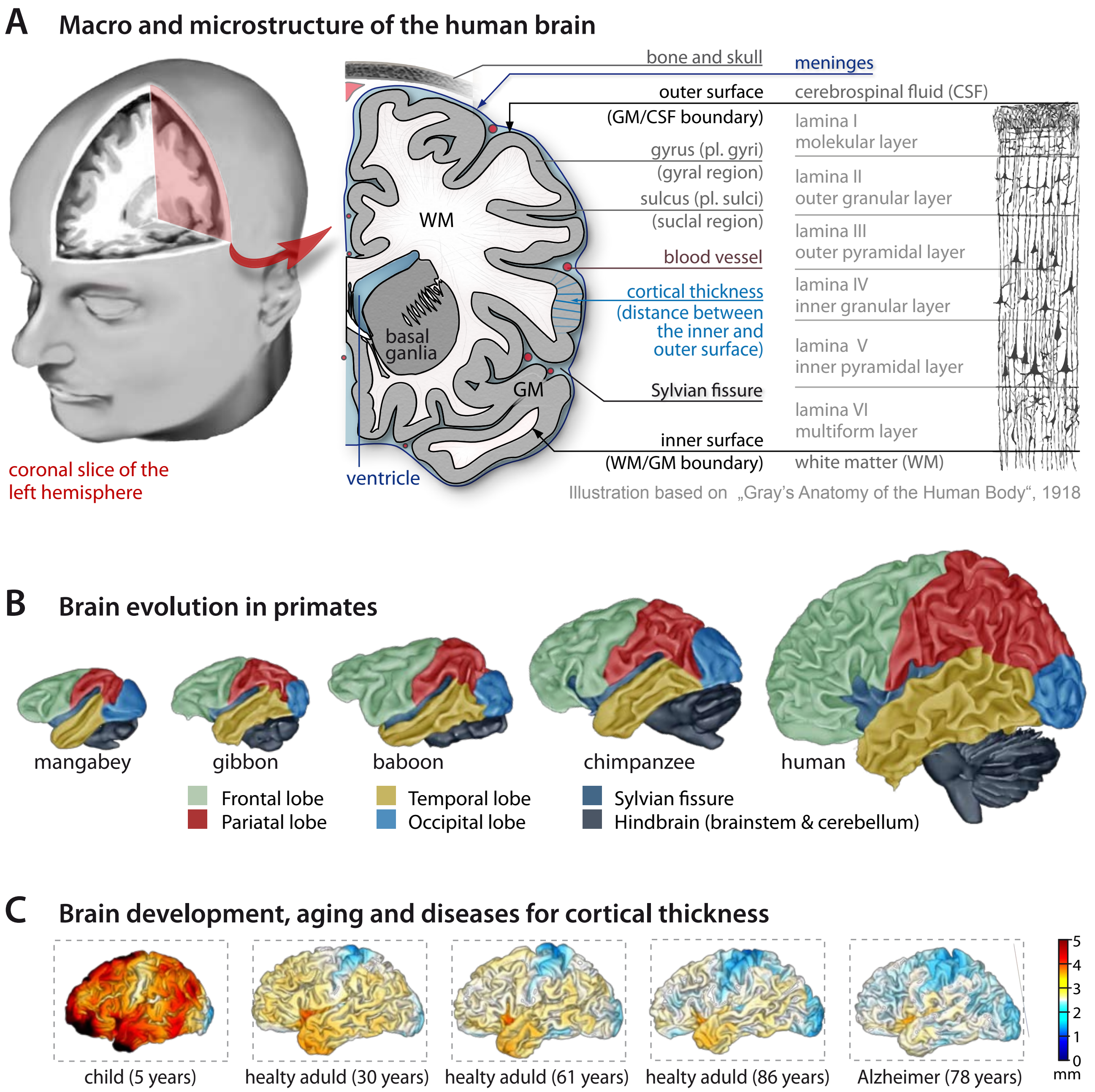

Figure 1: The human cerebrum (A) is a highly folded structure that can be macroscopically described as a ribbon of gray matter (GM) that surrounds a core of white matter (WM). This GM ribbon (neocortex) is around 2 to 4 mm thick and organized into six regions- and function-specific layers that contain different types of neurons and can be simply described as a processing region, whereas the WM is a high-speed connection between different brain regions. With increasing size, the brain evolves in a species-specific folding pattern (B) with increased individual influences (C) that occur early during an individual's development and stay relatively constant over an individual's lifetime, whereas other parameters such as thickness change significantly during development and aging (C).

variation in thickness and different functional processing. Its structure further depends on the local folding and compensate for the number of layer specific neurons, where imaginary cortical units contain the same amount of neurons per layer [1,5,13,20] (GM blocks A, B, C in Figure 2B). I.e., a cortical unit on top of a gyrus has a larger outer and smaller inner surface area with thicker inner and thinner outer layer (region C in Figure 2C), whereas a cortical unit on the bottom of a suclus has a smaller outer and larger inner surface area with thicker outer and thinner inner layer (region B in Figure 2C). It can therefore be expected that local folding only has a limited influence on function and can be seen as a simple product of energy-minimizing processes related to brain growth [14,15,19,21].

Magnetic resonance imaging (MRI) and automatic preprocessing techniques allow in vivo analysis of the macroscopic brain structure in the field of computational morphometry of even large cohorts [10,22]. Early regional manual measures were extended to automatic whole brain techniques such as voxel-based (VBM) [10], region-based (RBM) [23-25], deformation-based (DBM) [26], and surface-based morphometry (SBM) [12,22,23,27] that allow the detection of even subtle changes in the brain structure. In the last decade, the volume of the GM in particular as well as the cortical thickness has become an important biomarker for development [28], aging [29,30], plasticity [31], and a number of different diseases [32]. At this point, SBM allows essential improvements compared to VBM or DBM by (i) additional measures that describe the shape of the brain [18,33,34], (ii) dissection of GM volume into thickness and area [35], (iii) improved registration and partitioning (region alignment) [36], (iv) correct anatomical smoothing [32,37,38], (v) mathematical shape modeling [14,15,18,21,39], and (vi) combining different MRI modalities such as functional imaging (fMRI) that focuses on task-specific activation of cortical areas [38], diffusion imaging (dMRI) to analyze WM fiber tracts [40], and structural weightings such as T1, T2, PD, and quantitative imaging (qMRI) [41] to analyze tissue-specific properties such as myelination [42], WM hyperintensities or lesions in multiple-sclerosis [43]. Although VBM is very sensitive to subtle GM changes in brain plasticity, it lacks the function to describe complex folding pattern and its development, whereas DBM partially covers folding differences as well as volume changes that impede analysis. RBM on the other hand allows the combination of different techniques but depends on the atlas maps.

Prior to the technical description of surface reconstruction, modification, and measures, a small introduction to brain development, its underlying biomechanical processes, and modeling will be described here. *For a detailed introduction, see chapter 2.2 (development) and chapter 2.3 (normal aging).*

2. Brain development, plasticity, and aging

It is expected that brain folding follows the same biomechanical rules in all mammals, but the process itself is still undergoing significant research [6,8,9,14,19,44]. The development of the cerebrum undergoes three major periods: (i) the ballooning stage, (ii) the gyrification phase, and (iii) a subsequent scaling in childhood and adolescence. Further changes in the healthy adult brain are recognized as plasticity (short-time) and aging (long-time). The early ballooning phase is relatively similar between species including an enlargement by radial and tangential tissue growth (Figure 2), whereas gyrification is species-specific and shows higher tangential than radial growth that causes folding with more individual patterns in larger brains [8,9,14].

Phase I: ballooning

The ballooning phase from human gestation week (HGW) 0 to 15 is described by an intensive radial enlargement of the ventricle that compensates the simultaneous tangential growth of the intermediate zone and increases the brain surface without significant folding, where only the longitudinal and Sylvian fissures become prominent by bending . In HGW 5 to 20, neurons are generated in the ventricular zone a nd migrate to the skull, where they create the structure of the cortical layer. At this time, the cortex shows a radial dMRI pattern, indicating low connectivity within the cortex [9,14,44], with the first large fiber tracts becoming visible in the WM [40].

Phase II: gyrification

After ballooning and layer building, the neurons in the cortex start forming connections and the radial dMRI pattern gets lost [40]. Without intensive ventricular enlargement, the tangential growth becomes prominent and causes buckling . Gyrification starts with major structures such as the central sulcus [14]. External forces due to limitations of the skull and meninges were found to have minor effects [2,9,14,15,19], and it is presumed that gyrification depends on internal forces of WM connectivity (the axial tension theory [13]) or tangential growth of the GM (the buckling theory) [3,7]. Recent experimental and computational growth models [15,18,19,39] have shown promising results to explain the natural folding as an energy-minimizing process of surface expansion that relies on the stiffness of the inner core, the growing-rate, and local thickness, where thinner regions and faster growing rates increase folding and stiffer cores trigger more complex structures [15,19,39]. As far as the cortex, it has a lower limit of thickness of about 0.4 mm [6], gyrification generally only occurring for brains larger than 3 cm (about 10 cm3).

Phase III: further scaling

The folding is nearly completed around birth in humans [46] and both tangential and radial growth is balanced again [47], whereas gyrification starts after birth in other species such as ferrets [19].

Adulthood and aging

Over an individual's lifetime, the cortex shrinks slowly every year, whereas the WM continues to grow up to the age of around 40 years. The WM can show further degeneration as evidenced by MRI as WM hyperintensity with GM-like intensities in aging, as well as in diseases such as multiple sclerosis. Beside the global trend of tissue atrophy, brain plasticity allows an increase in local tissue volume. For elderly and people with neurodegenerative diseases such as Alzheimer's disease, accelerated tissue atrophy was reported [30]. Overall, tissue atrophy accompanies an enlargement of the ventricle and sulcal CSF that keeps the brain in a general shape within the skull.

Interim conclusion

Finally, we can conclude that the gyrification of the cortex in most mammals occurs most significantly during the second and third trimester of pregnancy most likely by local tangential growth of GM tissue after initial lamination at the end of the first trimester. As far as the fact that the folding pattern stays relatively constant over an individual's lifetime, it is expected to be possible to understand developmental processes and diseases even in the adult brain. *For further information about development and aging, refer to chapter 2.2 (development) and chapter 2.3 (normal aging).*

3. Folding theories and models

Folding processes can be found in most biological structures that require area enlargement, and it was shown that brain folding is also driven by biomechanical concepts that can be described by mathematical models [3,6,15,19]. It is assumed that the surface structure is driven by the organization of processing [13,18,48], that it is similar in mammals [6,8,9,19], and that folding abnormality such as lissencephaly or polygyria can help to understand the gyrification process [3,13,14,19]. A summary of mammal brain evolutional and abstract brain structure modeling is presented by Hofman [6], whereas a good introduction of up-to-date folding models can be found in previous reports [8,9,19]. There are two major types of gyrification theories: (i) the axonal tension theorem and (ii) the active growth models.

The axonal tension model [13] is based on the idea that neurological processing is more strongly correlated to gyri than sulci and that both sides of a gyrus are strongly connected by fibers

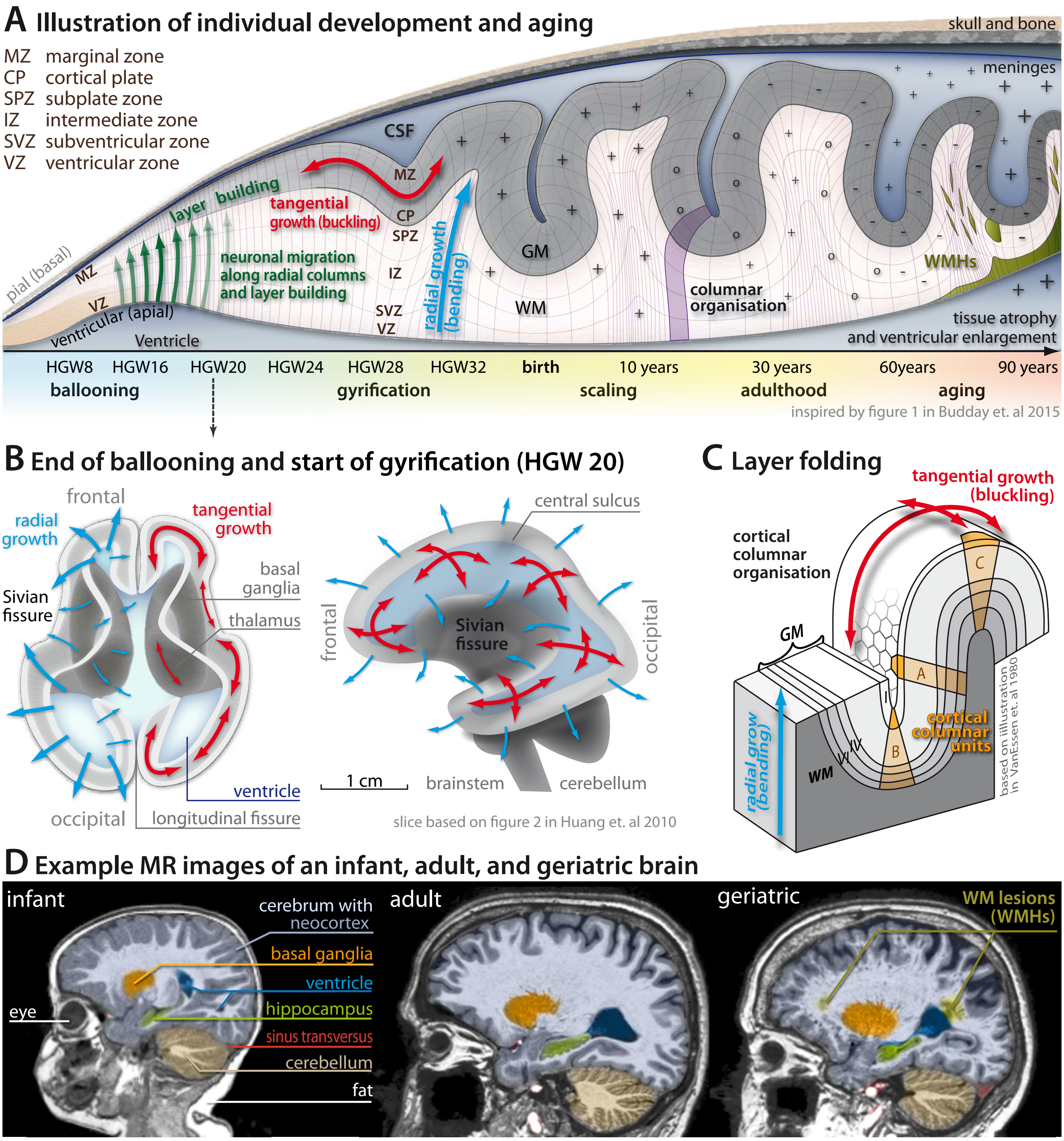

Figure 2: An illustration of human brain development and aging (A). It is initiated with the ballooning phase that strongly increases the area of the ventricular zone by both radial and tangential growth, where neuroepithelial cells are generated by cell division and migrate to the marginal zone forming a columnar migration and cortical layer pattern [1,5,45]. The ongoing migration and initiation of the cortical connection increase the tangential growth by about HGW 20 (B) and gyrification shapes major structures such as the central sulcus. Because the Sylvian fissure lies hidden behind the subcortical structures, such as the basal ganglia and the thalamus, it profits less from neuronal migration and is finally overgrown by the surrounding brain regions (B). In humans, gyrification has nearly finished around birth and radial and tangential growth is balanced again, leading to a scaling of brain size with tissue growth and surface area enlargement (A). Over an individual's life-time, the WM keeps growing up to the age of around 40 years, whereas the cortex shrinks slightly every year. In aging, the WM also shrinks and shows tissue degeneration that appears in MRIs as WM hyperintensities (WMHs) with GM-like intensities. Overall, the tissue atrophy is accompanied by an enlargement of the ventricle, that helps to keep the shape of the brain relatively constant. The local folding (bending and buckling) compresses and stretches the cortical layers shown in (C) by keeping the volumes of each layer of the imaginary cortical columnar units A, B, and C relatively similar and facilitates the increasing individual local folding pattern in higher species [1,5,45]. For comparison colorized real MR slices are shown in subfigure D.

that trigger the folding process to minimize connectivity costs. Although this theory looks elegant and has garnered support [17], it has four major drawbacks: (i) the predicted radial connections have not been observed macroscopically [19], rather in diffusion images [49], where most fibers run in radial direction, rather between the opposing sides of gyri, (ii) the predicted tension has not been observed in macroscopic cuts [21], (iii) perforation of the WM after neuronal migration and before the onset of gyrification did not lead to less folding [2], and finally (iv) mathematical folding models without the simulation of axonal fiber tensions [15,18] have proved to be successful.

In active growth models, cortical folding is just a side product of cortical enlargement and external and internal constraints [3,7,9,15,18,19,39]. In recent years, different computational folding models were introduced with varying combinations of radial and tangential growth [14,15,18,21,39,49], thickness [39], stiffness [19,39], growing speed [19], and external constraints such as the skull or meninges [9,49].

The work of Tallinen [15] was especially noteworthy and he investigated the development of specific folding patterns depending on WM stiffness, GM thickness, and the growing speed that allowed the creation of a naturally 3D folding pattern. It is further supported by the continuous work of the groups of Budday [14,39], Bayly [19], Toro [18], and Nie [49]. The idea of folding prediction based on real MRIs that allows validation by longitudinal studies in neonates is also remarkable [49].

4. Surface creation

The development of the brain as an organized surface has clearly outlined the potential of surface-based analysis, leading to the development of several software packages for automatic surface reconstruction and analysis of MRIs. Surface meshes are graph structures that describe a shape by a set of vertices V and faces F that connect the vertices. V is a nv × 3 vector of the xyz-coordinates of each point, whereas F describes the triangles by a nf × 3 vector of vertex-indices (Figure 3):

$$S = [V,F]. \tag{1}$$

Individual meshes can be generated on a regular volume grid by marching cubes or isosurface algorithms that generally require further pre- and post-processing. Surface measures are stored as vertex or face-wise vectors C that can be visualized as surface textures and analyzed similarly to VBM. Validation of surface reconstruction and measures is typically part of the method proposal and often includes simulated [50,51], scan-rescan [51], expert-classification 36, or large-scale datasets [52]. The quality of the generated meshes and measures depends on the method used [27], the reconstructed structure and region [11,20], as well as the quality of the input data [47,53]. In general, structural data that is suitable for VBM analysis also allows an adequate SBM analysis. The generation and analysis of surface measures will be part of sections 5 and 6, as the focus in this chapter is on mesh generation, modification, and mapping. Surfaces are usually generated using volumetric scans and require three major processing steps: (i) voxel-based preprocessing, (ii) the generation and optimization of individual meshes, and (iii) the registration to common templates (Figure 3A).

4.1. Voxel-based preprocessing

The voxel-based preprocessing is required to estimate mappings between individual and common brain templates (registration, see chapter 1.1), to classify different tissues (segmentation, see chapter 1.2) and prepare data for surface reconstruction.

The classification of WM, GM, and CSF is driven by image intensity and a priori knowledge [10,22,54] and generally comprehends the extraction of the brain [10,54], the handling of image interferences such as noise [10,55] and inhomogeneity [10], and in some cases also the registration [54]. Popular software packages such as BrainSuite , FSL , MIPAV, SPM [10,54], and VBM8/CAT applied common Gaussian-mixture, maximum-likelihood, maximum a posteriori probability, and expectation maximization models [10,40,54,56]. To increase accuracy and stability, recent approaches use brain-specific properties such as topological constrains [57], multimodal input images [10,54], longitudinal modeling [58], species or aging-specific templates and parameters [12,58], or other concepts entirely [59]. The segmentation can further be used for intensity normalization of MRIs [43].

Spatial registration estimates a mapping between the individual brain and common templates [60]. They are typically realized as iterative processes and start with affine transformations and low frequency deformations that are systematically increased to reduce the anatomical variance of the subjects [46]. Atlas maps that partition brains into different regions are often manually obtained in the native (subject) space and mapped to an average template space [24] or are directly generated in the template space [25]. Besides manual-defined atlas maps, automatic parceling methods e.g., fMRI and dMRI connectivity maps have also been suggested [61,62].

4.2. Mesh generation

Shape analysis requires surfaces with identical topology with the same faces and a similar number of vertices that can be achieved in two manners. The direct approach (top-down) uses an existing template mesh and deforms it to the individual anatomy [63-65]. This type of surface deformation works well for simple unfolded objects such as the skull [66], but runs into problems in the case of strongly folded structures [27]. Therefore, bottom-up methods dominate surface reconstruction with the creation of individual objects and registrations to an average mesh, typically a sphere [11,12,21,22,27,51,56,67,68].

Due to its wide set of cognitive function, the reconstruction of the neocortex of both cerebral hemispheres is most relevant and different reconstruction pipelines have been purposed, such as BrainSuite [69], BrainVoyager [68], Caret [12], CAT , ASP/CLASP [27,63], FreeSurfer [11], and MIPAV [67]. Most methods reconstruct the GM-WM inner/WM) surface that allows a better initial representation of the folded brain than the GM-CSF (outer/Pial) boundary that is often blurred in sulcal regions [22,27,56,63,67,68,70]. They fixed and optimized the mesh topology and deformed it to the CSF-GM boundary to estimate cortical thickness [27,37,63,71]. Some methods prefer the central surface to represent the cortex [12,51,67]. The central surface runs in the middle of the cortex and is the average of the inner and outer surface and is therefore less noisy compared to either the inner or outer surface.

Another approach is applied by BrainVisa that uses the WM surface to create independent surfaces of the major sulci to estimate and compare their morphology [48,69]. Besides the cortex, reconstruction of other brain structures such as ventricles [72], hippocampi [73], basal ganglia [73], or fiber tracts [74] have been proposed.

4.3. Mesh modification

The modification of surface meshes is required to optimize the initial meshes, prepare the surface registration, and create modified meshes for specific shape measures. Surface meshes can be modified in different ways, with the most important including:

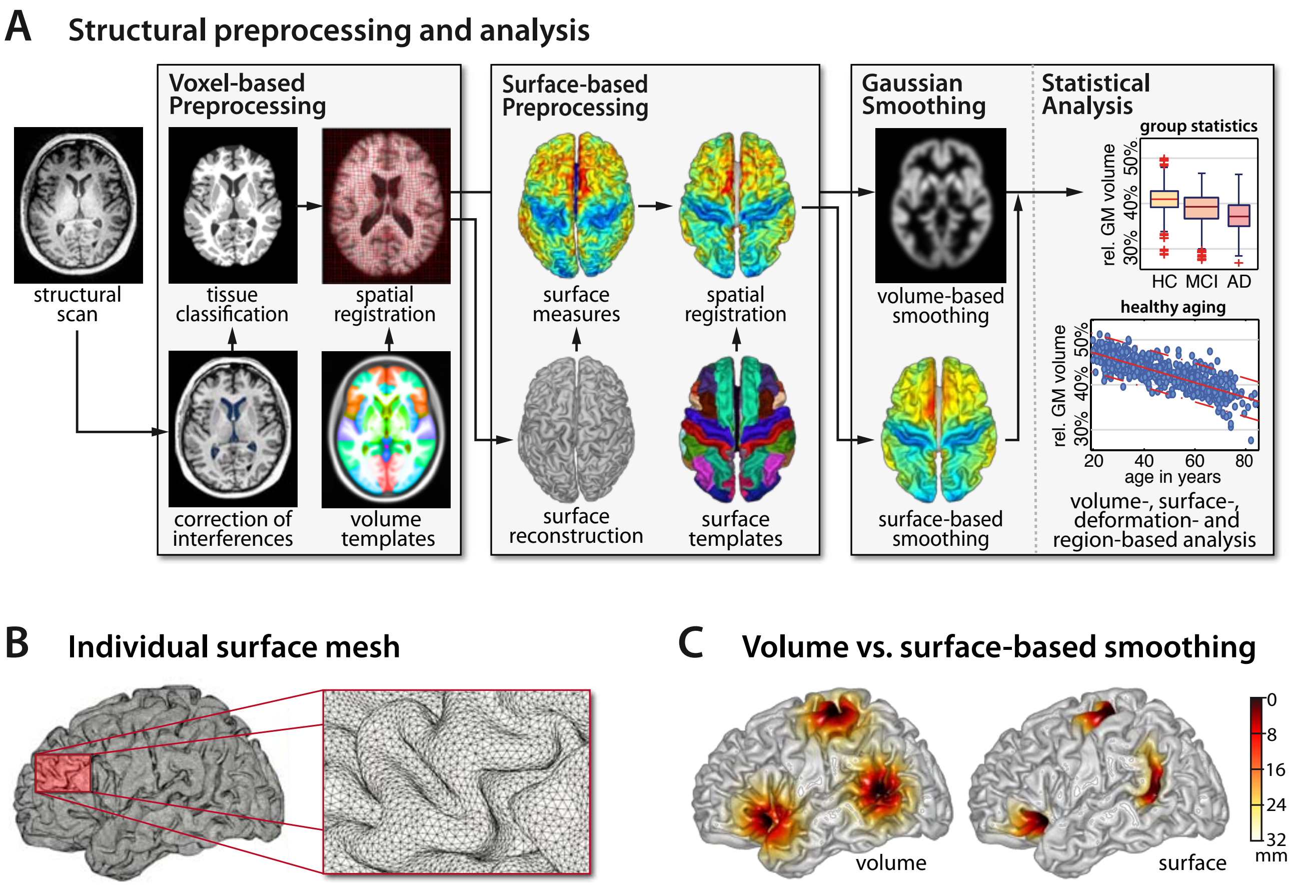

Figure 3: The preprocessing of structural MRIs often contains a voxel-based part that classifies the tissues and registers each brain to a template (A). The processed images support the reconstruction of surfaces that facilitates further surface-based measures. Similar to the voxel-based processing, a registration to a template mesh is required. For the final analysis, the VBM, DBM, and SBM data are smoothed to reduce individual variance and guarantee Gaussian distribution for statistical testing or average region-wise RBM analysis. (B) Surface meshes consist of vertices that are connected by faces and include multiple surface measures. (C) Smoothing on the surfaces is closer to the anatomical structure of the cortex and can improve analysis, especially in regions with deep folds [32,37].

(a) smoothing and inflation, (b) deformation, (c) remeshing, (d) decomposition, and (e) averaging (see Figure 4).

(a) Smoothing and inflation

Smoothing of mesh geometry reduces noise and artifacts by averaging the coordinates of neighbored vertices. At the same time, it removes anatomical details and unfolds the surface with growing number of iterations [12,37,75].

(b) Deformation

The movement of mesh vertices (deformation) allows small refinements by anatomical details, e.g., to handle longitudinal changes [49,64], midscale deformation such as the transformation of the brain surface position (e.g., from the GM-WM to the GM-CSF boundary [22,27,56,67,70]), as well as large changes such as the transformation from one individual surface to another one [63,65,66]. The deformation is controlled by internal (e.g., mesh connectivity) and external forces (e.g., vector fields based on image intensity).

(c) Remeshing and Repairing

Remeshing describes the modification of the mesh structure by resolution and topology changes. Remeshing algorithms can reduce or increase the number of vertices and faces by preserving geometry, topology, and other properties to optimize computational and anatomical constrains, e.g., to guarantee a uniform sampling distance of the mesh after topology correction or deformation [76]. Due to noise, artifacts, blood vessels, and resolution limits, the initial surface often contains topological defects (holes and handles), islands (unconnected components), singular vertices or complex edges, gaps, overlaps, intersections, or inconsistent orientations that require repairing by geometrical or topological correction of the mesh [68,77].

(d) Parameterization

The Fourier analysis and synthesis describes the representation, approximation, and reconstruction of signals by sums of simpler (trigonometric) functions. It allows the application of spherical harmonics (a fast Fourier transformation on the sphere) for objects that can be simplified as a folded sphere such as the cortical hemispheres [33,78]. The fraction of specific frequency can be used for shape characterization 78, specific folding measures (see section 4.5), and to remove specific frequency patterns (e.g., artifacts) [33,77].

(e) Averaging

After surface registration (see next section), the relations between the vertices of multiple meshes allow the creation of an average mesh with the topology of one of the meshes and a mix of the coordinates of the linked vertices [63,67,75]. The average mesh can be used for folding measures, data representation, and visualization.

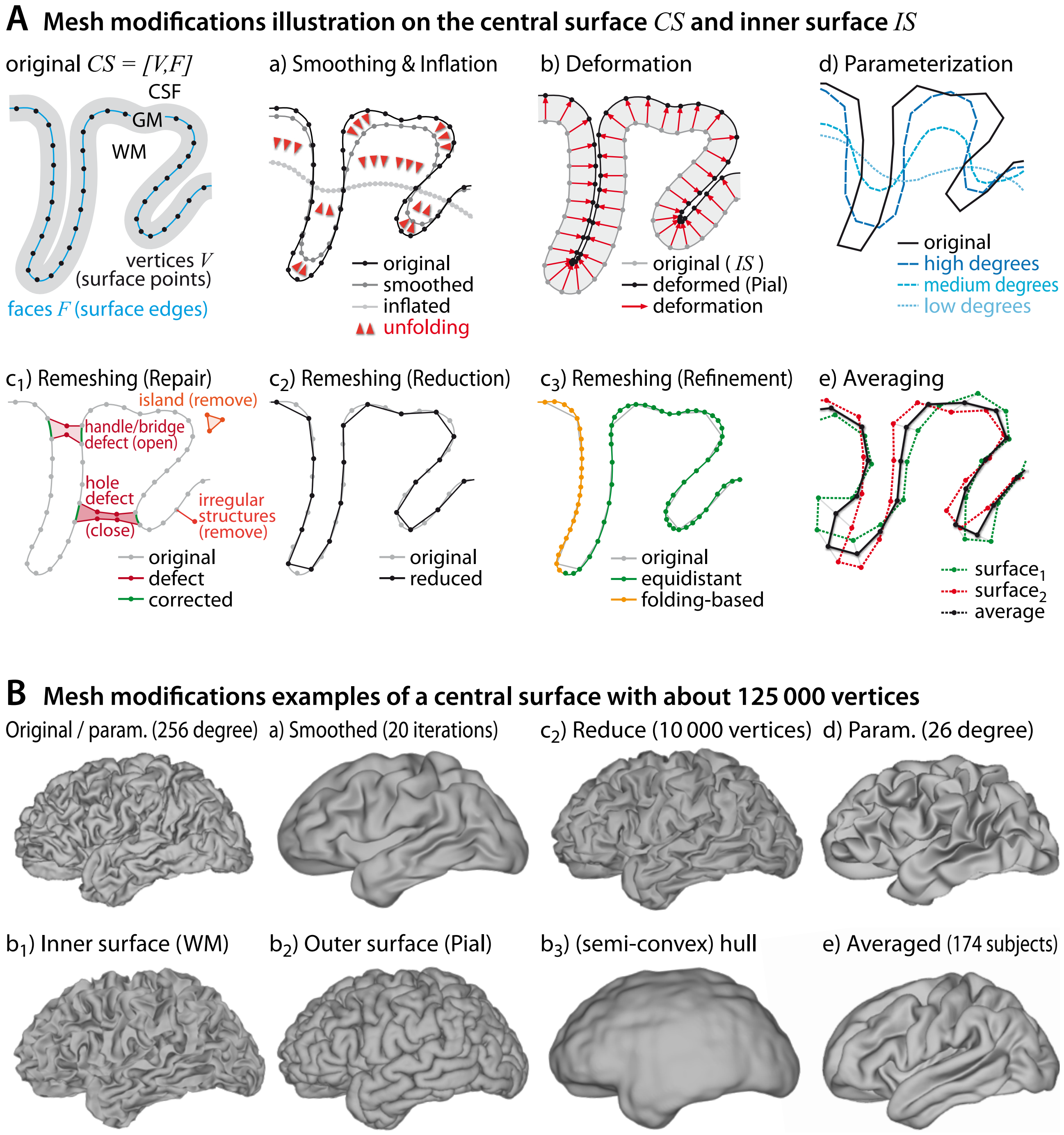

Figure 4: The surface creation and many shape measures require modification of the surface, e.g., to create smoother unfolded versions, repair the topology, or reduce the resolution for faster processing. The most typical operations are illustrated here for the central surface CS in 2D (A) and 3D (B): smoothing averages the coordinates of each vertex with its neighbors and remove artifacts, anatomical details, or the folding pattern (a). Deformation moves the vertices based on internal (e.g., mesh connectivity) and external forces (e.g., tissue intensities) (b). Remeshing (reduction/refinement/repair) changes the complexity and topology of the mesh (c). Parameterization comprises the analysis and synthesis of signals by sums of simpler trigonometric functions (d). Averaging mix normalized meshes with different vertex positions but identical structures to create a common mesh (e).

4.4. Spatial normalization and spherical registration of meshes

To compare individual meshes, a stable mapping to a common template (e.g., a sphere) is required [16,36,75]. The surface registration is the minimization of surface properties and shape features for small (intra-individual) [28], medium (inter-individual) [16,36,75], or large (inter-species) folding patterns [16]. Although voxel-based registration works with high accuracy, surface-based registration profits by the improved characterization of the cortex by surface measures and matching techniques with advanced alignment of individual structures.

4.5. Surface measures

There are various ways to describe structural properties of one or more multiple shapes: (a) projection of volumetric data, (b) (cortical) thickness, (c) surface relations, (d) curvature, (e) depth, (f) (span) width, (g) parameterization, and (h) landmarks (see Figure 5).

(a) Value extraction

The extraction of intensity can be used to process volumetric data from different MRI-modalities such as T1, T2, PD, dMRI, qMRI, or fMRI at different layer-specific positions, e.g., to characterize local myelinization [42], fiber orientation (DTI tensor field vs. surface normal) [79], fiber density [80], or tract geometry [81]. *For further information and discussion, see chapter 2.4 (cytoarchitectonic tissues and MRI-based signal intensities).*

(b) Thickness

One of the best known and most frequently used shape measures is the cortical thickness (sometimes also named cortical depth) that describes the width of the GM ribbon as the voxel- or surface-based distance between the inner and outer boundary. There are multiple metrics to estimate the thickness, most important are the (average) nearest neighbor T_{near} (FreeSurfer) [37,63,71], the surface normal T_{normal} [63], the coupled surface T_{link} [27,37,63], the Eikonal $T_{Eikonal}$ [51,67], and the Laplacian metric $T_{Laplacian}$ [51,82]. Although these metrics lead to slightly different results that should not be confused, similar patterns have been observed [2, 9,32,35,51,52,63,80,83]. *For further information and discussion, see chapter 1.2 (cortical thickness).*

(c) Surface relations

The complexity of a shape can be measured in relation to simplified unfolded version(s) with removed local details by (i) smoothing, (ii) morphologic operations such as closing or opening, (iii) averaging, (iv) down-sampling, or (v) other low-frequency representations such as spherical harmonics [84]. The most famous surface relation-based complexity measures are the gyrification index (GI) and the fractal dimension (FD).

The GI was first defined as the relation between the length of the folded contour and its envelope contour within a slice 85. With growing computational possibilities, the GI was automated regional surface-based [86] and continuous surface-based measures [18,87]. The GI was applied in the context of evolution [17], development, aging, and diseases [18].

The FD is a complexity ratio that describes how details in a pattern change with the scale at which it is measured [88]. The classic example is given by measuring the coastline of England that increases with finer scaling, recording more and more local details. In a similar way, the cortical folding of the brain can be partially characterized by describing the local enlargements by increased folding [89]. The FD of the brain can be defined by reducing volume [89] or mesh resolution [84]. FD has been applied to normal development and aging [89], as well as in the context of diseases [84].

The principle advantage of these measures is the intrinsic handling of the object size that allows simple comparisons for different individual and evolutional development stages [85,88]. Interestingly, GI and FD end up with a similar complexity of about 2.5 for the human brain [84,87].

(d) Curvature

The local curvature of a surface can be illustrated in 2D as a circle that fits the local contour. In 3D, the so-called principal curvatures are estimated for each vertex and allow the definition of a wide set of folding measures, with the four most prominent: (i) the (absolute) mean curvature [90,91], (ii) the Gaussian curvature [86,90], (iii) the shape index [90], and (iv) the curvedness [90]. In most cases, the cortical curvature is described as the average of the curvature of the inner and outer surface that is equivalent to the curvature of the central surface [91]. Because the principle curvatures depend on brain size [78,91], more complex measures try to incorporate normalization factors [86,90]. Nevertheless, most curvature measures correlate strongly, and restriction to the best fitting and simplest measures is recommended. Curvature measures were successfully used to describe changes in normal development, aging, and various diseases [86,90,91].

(e) Depth

The brain surface can be seen as a 3D signal [84] and its folding can be described by its frequency and amplitude. The amplitude can be characterized as the distance to a simplified surface, typically the hull surface of each hemisphere [82]. Similar to thickness, multiple distance metrics are available: the nearest neighbor [16], the Eikonal [67], the Laplacian [82], and the geodesic distance metric [92]. The nearest neighbor metric can cross sulci and gyri and therefore have lower values (especially in the Sylvian fissure), whereas the geodesic distance have the highest values [92]. Sulcal depth changes have been found in normal development, aging, and in various diseases [92].

(f) (Span)width

Besides the sulcal depth as a folding amplitude, the frequency of folds is also an interesting parameter that allows various measures including width, span, diameter, or thickness that describe the full or half distance between two sides of a gyrus or sulcus [6,83,93]. The width of the WM of a gyrus describes the local amount of myelinated fibers and how strong a region is connected to other regions [83], whereas the width of the CSF within a sulcus facilitates the investigation of local atrophy of WM and GM [93].

(g) Parameterization

A more abstract way of describing the folding is given by the spectral analysis of shape features [46,78]. Even complex signals can be described by simpler signals, e.g., the decomposition into a set of cosine or sine waves of different wavelength. This can be done by analyzing stepwise unfolded versions of the surface by Laplace-Beltrami [94], Spherical Harmonic [33,34,84], or Wavelet decomposition [34]. The spectral analysis of shape features allows a focus on specific spatial frequency bands that give the most important information to describe differences in the folding pattern [46,78], where especially the second and third folding degree is relevant and not the basic shape of the brain or head [78]. It is important to mention that low folding reconstruction (Fourier synthesis, see Figure 4B) creates an abstract pattern that supports no straightforward interpretation, e.g., as a development pattern [95]. Parameterization has been applied in the context of development, aging, and various diseases [46,78].

(h) Landmarks

Besides global and continuous measurement, the subdivision of the cortex into gyral and sulcal regions [62,96], or the extraction of surface landmarks such as sulcal bottom lines and pits, or gyral crones and peaks [97-99] were developed to support region-based analysis [69,96], to extract further anatomical features [97,98], or to improve registration accuracy [36]. The classification of special regions and structures can be further improved by other modalities such as dMRI 61 and fMRI [62]. In particular, BrainVisa focuses on the analysis of sulcal surfaces and allows the estimation of sulcus-specific measures of length, width, and folding [23,93,99].

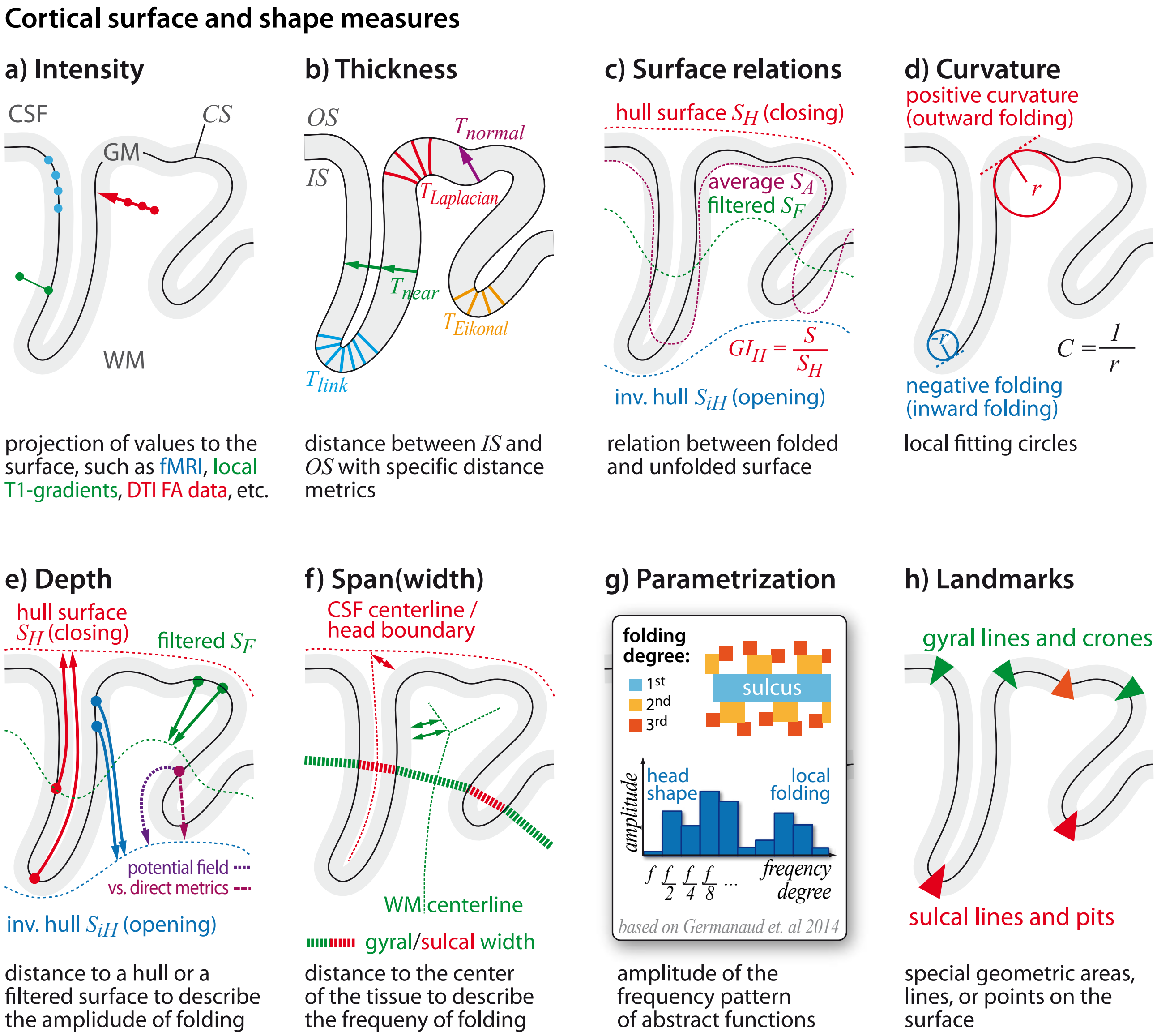

Figure 5: Conceptual surface measures: (a) intensity, (b) thickness, (c) surface relation, (d) curvature, (e) depth, (f) span(width), (g) parameterization, and (h) landmarks. Shown is the 2D illustration of the central (CS), inner (IS), outer surface (OS), and unfolded versions such as the hull surface SH, its counterpart SiH, and the filtered unfolded surface SF.

Interim conclusion

There are many approaches that describe different properties of the surface shape, reflecting new opportunities, as well as challenges for morphologic brain analysis, due to overlapping and similar measures, variable dependency of brain size (scaling invariance), and highly abstract measures that do not allow straightforward interpretation. A clear theory about the anatomical background of shape changes and the behavior of the applied measures is therefore essential.

4.6. Surface analysis (SBM)

Surface analysis, especially the cortical thickness and folding measures, have become an important aspect of structural brain imaging. Similar to VBM, SBM can be evaluated globally, by regions, or continuously over the whole surface. Beyond that, it allows new and more subtle measures, anatomical correct registration and smoothing, and direct interaction with mathematical folding models.

In the previous chapter, several different types of surface measures were introduced. In particular, shape measures allow questions to be answered that VBM does not support. SBM allows the simplified decomposition of the GM volume VGM into surface area AGM and thickness TGM:

$$\mathrm{VGM} = \mathrm{AGM} \cdot \mathrm{TGM}, \quad (2)$$

where the local folding can be neglected due to the expected compensation by the alteration of the cortical layers 1,13,20. The decomposition of volume is especially important in brain development, with increasing surface area (tangential growth), but decreasing cortical thickness due to WM formation that impedes GM volume analysis.

The cortex is an organized surface [13,18,48] making surface registration preferable compared to volume-based methods. Besides, the registration and, in particular, the smoothing benefit from the surface-based organization of the brain, where the surface distance between the top of opposing gyri is in most cases more than twice the direct distance [32,37,38] and a typical 8 mm volume-based smoothing blurred opposing sulci and gyri [37,71,75] (see Figure 3). Smoothing has the general effect of rendering the data to be more normally distributed and thereby increases the validity of the subsequent statistical tests and reduces outliers by noise, artifacts, or preprocessing errors [32,37,38].

Recent computational folding models demonstrated that gyrification depends on surface properties and that such models are capable of forecasting individual folding pattern development [15,18,19,39,49]. Hence, they also predict which circumstances lead to current folding patterns and can be used to understand developmental diseases such as autism spectrum disorder, or schizophrenia [18,84]. Surface measures are therefore an important source of validating and improving cortical folding models. On the other hand, folding models can help to refine surface generation by further constraints or improve brain phantoms such as the brain web phantom [50] by supporting anatomical changing (longitudinal) phantoms for method evaluation.

The major drawbacks of SBM are: (i) the high complexity, which makes it vulnerable to noise, artifacts, and errors, (ii) the considerable computational demands, and (iii) the sophisticated interpretation of some folding measures. Surface preprocessing is more complex and therefore in general more error-prone and it is expected to be less sensitive (due to its constraints), as well as less robust (because of its complexity), especially for subtle changes in brain plasticity. On the other hand, constraints can improve the robustness and the increased complexity comes along with more characteristic measures, anatomical advanced registration and smoothing that may compensate this handicap [35,84]. Because of the high amount of available measures, the challenge is to focus on measures that describe the expected changes or the use of big data techniques. A general limit of some gyrification measures is given by the arbitrary definition of unfolded structures, different metrics, and normalization factors. Many folding measures use unfolded structures that include the Sylvian but not the inter-hemispheric fissure, which might therefore bias the results. Furthermore, some folding measures are limited in describing the correct localization of changes that depend on deep WM tracts or the ventricle. Different metrics, e.g., for thickness or curvature, lead to slightly varying results, that limit the comparisons of different studies. It is also relevant to know if the used measures are intrinsic scaling invariant such as most relation measures that compare a folded and unfolded surface of the same subject, in contrast to most absolute measures, such as thickness, curvature, folding depth, and width, that depend on brain size and require covariates such as the total intra-cranial volume (TIV) for scaling normalization in the analysis [83].

Similar to VBM, SBM relies on the quality of the original data, with recent studies showing a clear influence of image quality on structural measures, with lower quality leading to GM underestimation 100 making quality assurance an important side aspect of the analysis [47,53].

4.7. Conclusion

Shape properties are one of the key factors to understand the causes and effects of individual and evolutional folding development [14,15,18,19,21,22]. Because folding is mostly affected by early development, shape measures have a high potential to investigate developmental dysfunctions even in the adult brain. Surfaces come along with a wide set of new or improved measures and an anatomical convenient registration and smoothing model. The description of surface characteristics by surface measures is essential for enhanced mathematical folding models that can simultaneously improve surface reconstruction, measures, and their validation [15,18,19,84]. Surface analysis offers a number of new measures with various definitions and properties that require careful evaluation, especially of abstract shape measures [46,78,84].

References

1 Bok, S. T. Der Einfluss der in den Furchen und Windungen auftretenden Krümmungen der Grosshirnrinde auf die Rindenarchitektur. Zeitschrift für die gesamte Neurologie und Psychiatrie 121, 682-750, doi:10.1007/BF02864437 (1929).

2 Barron, D. H. An experimental analysis of some factors involved in the development of the fissure pattern of the cerebral cortex. Journal of Experimental Zoology 113, 553-581, doi:10.1002/jez.1401130304 (1950).

3 Richman, D. P., Stewart, R. M. & Hutchinson, J. W. Mechanical mode of brain convolutional development. Science 189 (1975).

4 Mietchen, D. & Gaser, C. Computational morphometry for detecting changes in brain structure due to development, aging, learning, disease and evolution. Frontiers in Neuroinformatics (2009).

5 Rakic, P. Evolution of the neocortex: a perspective from developmental biology. Nature reviews Neuroscience 10, 724-735, doi:10.1038/nrn2719 (2009).

6 Hofman, M. A. On the evolution and geometry of the brain in mammals. Progress in neurobiology 32, 137-158 (1989).

7 Welker, W. in Why Does Cerebral Cortex Fissure and Fold? Vol. 8B 3-136 (Springer US, 1990).

8 Lewitus, E., Kelava, I. & Huttner, W. B. Conical expansion of the outer subventricular zone and the role of neocortical folding in evolution and development. Frontiers in Human Neuroscience 7, doi:10.3389/fnhum.2013.00424 (2013).

9 Striedter, G. F., Srinivasan, S. & Monuki, E. S. Cortical Folding: When, Where, How, and Why? Annual Review of Neuroscience 38, 291-307, doi:10.1146/annurev-neuro-071714-034128 (2015).

10 Ashburner, J. & Friston, K. J. Voxel-based morphometry--the methods. NeuroImage 11, 805-821, doi:10.1006/nimg.2000.0582 (2000).

11 Fischl, B. R. FreeSurfer. NeuroImage 62, 774-781, doi:10.1016/j.neuroimage.2012.01.021 (2012).

12 Van Essen, D. C. et al. An integrated software suite for surface-based analyses of cerebral cortex. Journal of the American Medical Informatics Association : JAMIA 8, 443-459 (2001).

13 Van Essen, D. C. A tension-based theory of morphogenesis and compact wiring in the central nervous system. Nature 385, 313-318, doi:10.1038/385313a0 (1997).

14 Budday, S., Steinmann, P. & Kuhl, E. Physical biology of human brain development. Frontiers in Cellular Neuroscience 9, 257, doi:10.3389/fncel.2015.00257 (2015).

15 Tallinen, T. et al. On the growth and form of cortical convolutions. Nature Physics, doi:10.1038/nphys3632 (2016).

16 Van Essen, D. C. Surface-based approaches to spatial localization and registration in primate cerebral cortex. NeuroImage 23 Suppl 1, S97-107, doi:10.1016/j.neuroimage.2004.07.024 (2004).

17 Hilgetag, C. C. & Barbas, H. Role of mechanical factors in the morphology of the primate cerebral cortex. PLoS computational biology 2, e22, doi:10.1371/journal.pcbi.0020022 (2006).

18 Toro, R. On the possible shapes of the brain. Evolutionary Biology (2012).

19 Bayly, P. V., Taber, L. A. & Kroenke, C. D. Mechanical forces in cerebral cortical folding: a review of measurements and models. Journal of the mechanical behavior of biomedical materials 29, 568-581, doi:10.1016/j.jmbbm.2013.02.018 (2014).

20 Amunts, K. & Zilles, K. Architectonic Mapping of the Human

Brain beyond Brodmann. Neuron 88, 1086-1107, doi:10.1016/j.neuron.2015.12.001 (2015).

21 Xu, G. et al. Axons pull on the brain, but tension does not drive cortical folding. Journal of Biomechanical Engineering 132, 071013, doi:10.1115/1.4001683 (2010).

22 Dale, A. M., Fischl, B. R. & Sereno, M. I. Cortical surface-based analysis. I. Segmentation and surface reconstruction. NeuroImage 9, 179-194, doi:10.1006/nimg.1998.0395 (1999).

23 Rivière, D. et al. Automatic recognition of cortical sulci of the human brain using a congregation of neural networks. Medical Image Analysis 6, 77-92 (2002).

24 Hammers, A. et al. Three-dimensional maximum probability atlas of the human brain, with particular reference to the temporal lobe. Human Brain Mapping 19, 224-247, doi:10.1002/hbm.10123 (2003).

25 Shattuck, D. W. et al. Construction of a 3D probabilistic atlas of human cortical structures. NeuroImage 39, 1064-1080, doi:10.1016/j.neuroimage.2007.09.031 (2008).

26 Gaser, C., Volz, H. P., Kiebel, S., Riehemann, S. & Sauer, H. Detecting structural changes in whole brain based on nonlinear deformations-application to schizophrenia research. NeuroImage 10, 107-113, doi:10.1006/nimg.1999.0458 (1999).

27 Kim, J. S. et al. Automated 3-D extraction and evaluation of the inner and outer cortical surfaces using a Laplacian map and partial volume effect classification. NeuroImage 27, 210-221, doi:10.1016/j.neuroimage.2005.03.036 (2005).

28 Li, G. et al. Measuring the dynamic longitudinal cortex development in infants by reconstruction of temporally consistent cortical surfaces. NeuroImage 90, 266-279, doi:10.1016/j.neuroimage.2013.12.038 (2014).

29 Fjell, A. M. et al. High consistency of regional cortical thinning in aging across multiple samples. Cerebral Cortex 19, 2001-2012, doi:10.1093/cercor/bhn232 (2009).

30 Ziegler, G., Ridgway, G. R., Dahnke, R., Gaser, C. & Initiative, A. a. s. D. N. Individualized Gaussian process-based prediction and detection of local and global gray matter abnormalities in elderly subjects. NeuroImage 97, 333-348, doi:10.1016/j.neuroimage.2014.04.018 (2014).

31 Maguire, E. A. et al. Navigation-related structural change in the hippocampi of taxi drivers. Proceedings of the National Academy of Sciences of the United States of America 97, 4398-4403, doi:10.1073/pnas.070039597 (2000).

32 Spjuth, M. S., Gravesen, F. H., Eskildsen, S. F. & Østergaard, L. R. Early detection of AD using cortical thickness measurements. Medical Imaging 6512, 65120L-65120L-65129, doi:10.1117/12.709806 (2007).

33 Shen, L. & Chung, M. K. Large-Scale Modeling of Parametric Surfaces Using Spherical Harmonics. International Symposium on 3D Data Processing, Visualization, and Transmission, 294-301 (2006).

34 Yu, P. et al. Cortical surface shape analysis based on spherical wavelets. IEEE Transactions on Medical Imaging 26, 582-597, doi:10.1109/TMI.2007.892499 (2007).

35 Winkler, A. M. et al. Cortical thickness or grey matter volume? The importance of selecting the phenotype for imaging genetics studies. NeuroImage, doi:10.1016/j.neuroimage.2009.12.028 (2009).

36 Tardif, C. L. et al. Multi-contrast multi-scale surface registration for improved alignment of cortical areas. NeuroImage 111, 107-122, doi:10.1016/j.neuroimage.2015.02.005 (2015).

37 Lerch, J. P. & Evans, A. C. Cortical thickness analysis examined through power analysis and a population simulation. NeuroImage (2005).

38 Anticevic, A. et al. Comparing surface-based and volume-based analyses of functional neuroimaging data in patients with schizophrenia. NeuroImage 41, 835-848, doi:10.1016/j.neuroimage.2008.02.052 (2008).

39 Budday, S., Raybaud, C. & Kuhl, E. A mechanical model predicts morphological abnormalities in the developing human brain. Scientific reports 4, 5644, doi:10.1038/srep05644 (2014).

40 Huang, H. Structure of the fetal brain: what we are learning from diffusion tensor imaging. The Neuroscientist 16, 634-649, doi:10.1177/1073858409356711 (2010).

41 Weiskopf, N. et al. Quantitative multi-parameter mapping of R1, PD(*), MT, and R2(*) at 3T: a multi-center validation. Frontiers in Neuroscience 7, 95, doi:10.3389/fnins.2013.00095 (2013).

42 Deoni, S. C. L., Dean, D. C., Remer, J., Dirks, H. & O'Muircheartaigh, J. Cortical maturation and myelination in healthy toddlers and young children. NeuroImage 115, 147-161, doi:10.1016/j.neuroimage.2015.04.058 (2015).

43 Shah, M. et al. Evaluating intensity normalization on MRIs of human brain with multiple sclerosis. Medical Image Analysis 15, 267-282, doi:10.1016/j.media.2010.12.003 (2011).

44 Jiang, X. & Nardelli, J. Cellular and molecular introduction to brain development. Neurobiology of disease, doi:10.1016/j.nbd.2015.07.007 (2015).

45 Van Essen, D. C. & Maunsell, J. H. R. Two-dimensional maps of the cerebral cortex. Journal of Comparative Neurology 191, 255-281, doi:10.1002/cne.901910208 (1980).

46 Wright, R. et al. Construction of a fetal spatio-temporal cortical surface atlas from in utero MRI: Application of spectral surface matching. NeuroImage 120, 467-480, doi:10.1016/j.neuroimage.2015.05.087 (2015).

47 Evans, A. C. & Group, B. D. C. The NIH MRI study of normal brain development. NeuroImage 30, 184-202, doi:10.1016/j.neuroimage.2005.09.068 (2006).

48 Régis, J. et al. „Sulcal root“; generic model: a hypothesis to overcome the variability of the human cortex folding patterns. Neurologia medico-chirurgica 45, 1-17 (2005).

49 Nie, J. et al. A computational growth model for measuring dynamic cortical development in the first year of life. Cerebral Cortex 22, 2272-2284, doi:10.1093/cercor/bhr293 (2012).

50 Collins, D. L. et al. Design and construction of a realistic digital brain phantom. IEEE Transactions on Medical Imaging 17, 463-468, doi:10.1109/42.712135 (1998).

51 Dahnke, R., Yotter, R. A. & Gaser, C. Cortical thickness and central surface estimation. NeuroImage 65, 336-348, doi:10.1016/j.neuroimage.2012.09.050 (2013).

52 Tustison, N. J. et al. Large-scale evaluation of ANTs and FreeSurfer cortical thickness measurements. NeuroImage, doi:10.1016/j.neuroimage.2014.05.044 (2014).

53 Poldrack, R. A. & Gorgolewski, K. J. Making big data open: data sharing in neuroimaging. Nature Neuroscience 17, 1510-1517, doi:10.1038/nn.3818 (2014).

54 Ashburner, J. & Friston, K. J. Unified segmentation. NeuroImage 26, 839-851, doi:10.1016/j.neuroimage.2005.02.018 (2005).

55 Coupé, P., Yger, P. & Barillot, C. Fast non local means denoising for 3D MR images. Medical Image Computing and Computer-Assisted Intervention 9, 33-40 (2006).

56 Shattuck, D. W. & Leahy, R. M. BrainSuite: an automated cortical surface identification tool. Medical Image Analysis 6, 129-142, doi:10.1016/S1361-8415(02)00054-3 (2002).

57 Bazin, P.-L. & Pham, D. L. Homeomorphic brain image segmentation with topological and statistical atlases. Medical Image Analysis 12, 616-625, doi:10.1016/j.media.2008.06.008 (2008).

58 Wang, L. et al. Longitudinally guided level sets for consistent tissue segmentation of neonates. Human Brain Mapping 34, 956-972, doi:10.1002/hbm.21486 (2013).

59 Mendrik, A. M. et al. MRBrainS Challenge: Online Evaluation Framework for Brain Image Segmentation in 3T MRI Scans. Computational intelligence and neuroscience 2015, 813696-813616, doi:10.1155/2015/813696 (2015).

60 Ou, Y., Akbari, H., Bilello, M., Da, X. & Davatzikos, C. Comparative Evaluation of Registration Algorithms in Different Brain Databases with Varying Difficulty: Results and Insights. IEEE Transactions on Medical Imaging, doi:10.1109/TMI.2014.2330355 (2014).

61 Anwander, A., Tittgemeyer, M., von Cramon, D. Y., Friederici, A. D. & Knösche, T. R. Connectivity-Based Parcellation of Broca's Area. Cerebral Cortex 17, 816-825, doi:10.1093/cercor/bhk034 (2007).

62 Schubotz, R. I., Anwander, A., Knösche, T. R., von Cramon, D. Y. & Tittgemeyer, M. Anatomical and functional parcellation of the human lateral premotor cortex. NeuroImage 50, 396-408, doi:10.1016/j.neuroimage.2009.12.069 (2010).

63 MacDonald, D., Kabani, N. J., Avis, D. & Evans, A. C. Automated 3-D extraction of inner and outer surfaces of cerebral cortex from MRI. NeuroImage 12, 340-356, doi:10.1006/nimg.1999.0534 (2000).

64 Nakamura, K., Fox, R. & Fisher, E. CLADA: Cortical longitudinal atrophy detection algorithm. NeuroImage 54, 278-289, doi:10.1016/j.neuroimage.2010.07.052 (2011).

65 Xu, C., Pham, D. L., Rettmann, M. E., Yu, D. N. & Prince, J. L. Reconstruction of the human cerebral cortex from magnetic resonance images. IEEE Transactions on Medical Imaging 18, 467-480, doi:10.1109/42.781013 (1999).

66 Smith, S. M. Fast robust automated brain extraction. Human Brain Mapping 17, 143-155, doi:10.1002/hbm.10062 (2002).

67 Tosun, D. et al. Cortical surface segmentation and mapping. NeuroImage 23 Suppl 1, S108-118, doi:10.1016/j.neuroimage.2004.07.042 (2004).

68 Kriegeskorte, N. & Goebel, R. An efficient algorithm for topologically correct segmentation of the cortical sheet in anatomical mr volumes. NeuroImage 14, 329-346, doi:10.1006/nimg.2001.0831 (2001).

69 Cachia, A. et al. A generic framework for the parcellation of the cortical surface into gyri using geodesic Voronoï diagrams. Medical Image Analysis 7, 403-416 (2003).

70 Eskildsen, S. F. & Ostergaard, L. R. Active surface approach for extraction of the human cerebral cortex from MRI. Medical Image Computing and Computer-Assisted Intervention 9, 823-830 (2006).

71 Fischl, B. R. & Dale, A. M. Measuring the thickness of the human cerebral cortex from magnetic resonance images. Proceedings of the National Academy of Sciences of the United States of America 97, 11050-11055, doi:10.1073/pnas.200033797 (2000).

72 Paniagua, B. et al. Lateral ventricle morphology analysis via mean latitude axis. Proceedings of SPIE--the International Society for Optical Engineering 8672, 86720M, doi:10.1117/12.2006846 (2013).

73 Qiu, A. & Miller, M. I. Multi-structure network shape analysis via normal surface momentum maps. NeuroImage 42, 1430-1438, doi:10.1016/j.neuroimage.2008.04.257 (2008).

74 Qiu, A. et al. Surface-based analysis on shape and fractional anisotropy of white matter tracts in Alzheimer's disease. PloS one 5, e9811, doi:10.1371/journal.pone.0009811 (2010).

75 Fischl, B. R., Sereno, M. I. & Dale, A. M. Cortical surface-based analysis. II: Inflation, flattening, and a surface-based coordinate system. NeuroImage 9, 195-207, doi:10.1006/nimg.1998.0396 (1999).

76 Frey, P. J. Anisotropic surface remeshing. (Elsevier, 2001).

77 Yotter, R. A., Dahnke, R., Thompson, P. M. & Gaser, C. Topological correction of brain surface meshes using spherical harmonics. Human Brain Mapping 32, 1109-1124, doi:10.1002/hbm.21095 (2011).

78 Germanaud, D. et al. Larger is twistier: spectral analysis of gyrification (SPANGY) applied to adult brain size polymorphism. NeuroImage 63, 1257-1272, doi:10.1016/j.neuroimage.2012.07.053 (2012).

79 Kleinnijenhuis, M. et al. Diffusion tensor characteristics of gyrencephaly using high resolution diffusion MRI in vivo at 7T. NeuroImage 109, 378-387, doi:10.1016/j.neuroimage.2015.01.001 (2015).

80 Nie, J. et al. Longitudinal development of cortical thickness, folding, and fiber density networks in the first 2 years of life. Human Brain Mapping 35, 3726-3737, doi:10.1002/hbm.22432 (2014).

81 Savadjiev, P. et al. Fusion of white and gray matter geometry: a framework for investigating brain development. Medical Image Analysis 18, 1349-1360, doi:10.1016/j.media.2014.06.013 (2014).

82 Jones, S. E., Buchbinder, B. R. & Aharon, I. Three-dimensional mapping of cortical thickness using Laplace's equation. Human Brain Mapping 11, 12-32 (2000).

83 Im, K. et al. Sulcal morphology changes and their relationship with cortical thickness and gyral white matter volume in mild cognitive impairment and Alzheimer's disease. NeuroImage 43, 103-113, doi:10.1016/j.neuroimage.2008.07.016 (2008).

84 Yotter, R. A., Nenadic, I., Ziegler, G., Thompson, P. M. & Gaser, C. Local cortical surface complexity maps from spherical harmonic reconstructions. NeuroImage 56, 961-973, doi:10.1016/j.neuroimage.2011.02.007 (2011).

85 Zilles, K., Armstrong, E., Schleicher, A. & Kretschmann, H.-J. The human pattern of gyrification in the cerebral cortex. Anatomy and Embryology 179, 173-179, doi:10.1007/BF00304699 (1988).

86 Rodriguez-Carranza, C., Mukherjee, P., Vigneron, D. B., Barkovich, A. J. & Studholme, C. A framework for in vivo quantification of regional brain folding in premature neonates. NeuroImage 41, 462-478, doi:10.1016/j.neuroimage.2008.01.008 (2008).

87 Schaer, M. et al. A surface-based approach to quantify local cortical gyrification. IEEE Transactions on Medical Imaging 27, 161-170, doi:10.1109/TMI.2007.903576 (2008).

88 Mandelbrot, B. How long is the coast of britain? Statistical self-similarity and fractional dimension. Science 156, 636-638, doi:10.1126/science.156.3775.636 (1967).

89 Jiang, J. et al. A robust and accurate algorithm for estimating the complexity of the cortical surface. Journal of Neuroscience Methods 172, 122-130, doi:10.1016/j.jneumeth.2008.04.018 (2008).

90 Pienaar, R., Fischl, B. R., Caviness, V. S., Makris, N. & Grant, P. E. A methodology for analyzing curvature in the developing brain from preterm to adult. International Journal of Imaging Systems and Technology (2008).

91 Luders, E. et al. A curvature-based approach to estimate local gyrification on the cortical surface. NeuroImage 29, 1224-1230, doi:10.1016/j.neuroimage.2005.08.049 (2006).

92 Yun, H. J., Im, K., Yang, J.-J., Yoon, U. & Lee, J.-M. Automated sulcal depth measurement on cortical surface reflecting geometrical properties of sulci. PloS one 8, e55977, doi:10.1371/journal.pone.0055977 (2013).

93 Kochunov, P. V. et al. Relationship among neuroimaging indices of cerebral health during normal aging. Human Brain Mapping 29, 36-45, doi:10.1002/hbm.20369 (2008).

94 Levy-Cooperman, N., Ramirez, J., Lobaugh, N. J. & Black, S. E. Misclassified tissue volumes in Alzheimer disease patients with white matter hyperintensities: importance of lesion segmentation procedures for volumetric analysis. Stroke 39, 1134-1141, doi:10.1161/STROKEAHA.107.498196 (2008).

95 Shishegar, R., Britto, J. M. & Johnston, L. A. in Conference proceedings : Annual International Conference of the IEEE Engineering in Medicine and Biology Society IEEE Engineering in Medicine and Biology Society Conference Vol. 2014 1525-1528 (2014).

96 Desikan, R. S. R. et al. An automated labeling system for subdividing the human cerebral cortex on MRI scans into gyral based regions of interest. NeuroImage 31, 968-980, doi:10.1016/j.neuroimage.2006.01.021 (2006).

97 Li, G., Guo, L., Nie, J. & Liu, T. Automatic cortical sulcal parcellation based on surface principal direction flow field tracking. NeuroImage 46, 923-937, doi:10.1016/j.neuroimage.2009.03.039 (2009).

98 Meng, Y., Li, G., Lin, W., Gilmore, J. H. & Shen, D. Spatial distribution and longitudinal development of deep cortical sulcal landmarks in infants. NeuroImage 100, 206-218, doi:10.1016/j.neuroimage.2014.06.004 (2014).

99 Hopkins, W. D. et al. Evolution of the central sulcus